

1 STUDY SITES

1 To accurately estimate and validate the ice volume of AIR the model requires three kinds of datasets
2 namely, weather, water and ice volume. So through the winters of 2019, 2020 and 2021 several scientific
3 AIR were constructed by teams in Switzerland and India. Each site had an Automatic Weather Station
4 (AWS) nearby. Also drone flights were conducted periodically to record AIR ice volume. For this analysis,
5 we have chosen 4 of the AIR which have a relatively complete dataset associated with them.

6 1.1 Construction

7 The construction strategy used in each site varied. CH20 and CH21 AIR was constructed on a garden
8 adjacent to a stream. To initiate the ice formation process, tree branches were laid covering the fountain
9 pipe. The fountain height varied between 2 to 5 m during the construction period. Fountain operation was
10 guided by temperature conditions.

11 The IC21 AIR was constructed adjacent to another AIR and merged with it. To initiate the ice formation
12 process, a dome of 2 m radius was constructed and the fountain pipeline was erected at the center using a
13 tripod. Fountain operation was interrupted only due to pipeline freezing events. The fountain height varied
14 between 5 to 9 m.

15 The EP19 AIR was constructed inside a wooden boundary adjacent to a stream. Fountain operation was
16 guided by temperature conditions. The water spray of the fountain was initially adjusted so that most of
17 the water droplets land within the wooden boundary zone. The ice formation was guided by adding a
18 metal framework at the ice structure base after the first night of operation. Several cotton threads were tied
19 between the ice structure base and fountain pole for accelerating and further guiding the ice formation
20 process.

21 1.2 Measurements

22 1.2.1 Weather measurements

23 Air temperature, relative humidity, wind speed, pressure, longwave, shortwave direct and diffuse radiation
24 are required to calculate the surface energy balance of an AIR. All the 4 sites had AWS near the construction
25 site which measured most of these parameters. The specific corrections applied on the input dataset for
26 each site is described in the Appendix. In addition, we used ERA5 reanalysis dataset (Copernicus Climate
27 Change Service (C3S), 2017) for filling data gaps and adding data that were not measured directly at the
28 respective site. The ERA5 reanalysis dataset has a good correlation with lower elevation sites in Switzerland
29 (Scherrer, 2020) but a poor correlation for the Indian (IN21) site. So the weather dataset for the IN21 site
30 was completed using another AWS nearby as described in the Appendix.

31 1.2.2 Discharge measurements

32 The water flow rate or discharge was measured via an ultrasonic sensor attached to the fountain
33 supply pipeline for all the sites. However, due to various malfunctions, the discharge measurements
34 were incomplete for all the sites except CH19. Using the hourly webcam images of the CH sites, the
35 discharge duration was determined. The available discharge measurement was later used to determine the
36 average discharge quantity during these periods.

37 1.2.3 Ice volume measurements

38 Several Drone flights were conducted in every AIR site. The DEM generated through these flights were
39 analysed to obtain the circumference and volume of the ice structure. The mean circumference measured
40 during the fountain duration was set as the spray radius (r_{spray}) and the first drone flight was used to set
41 the dome volume (V_{dome}) for model initialisation. The ice volume data was later used for calibration and

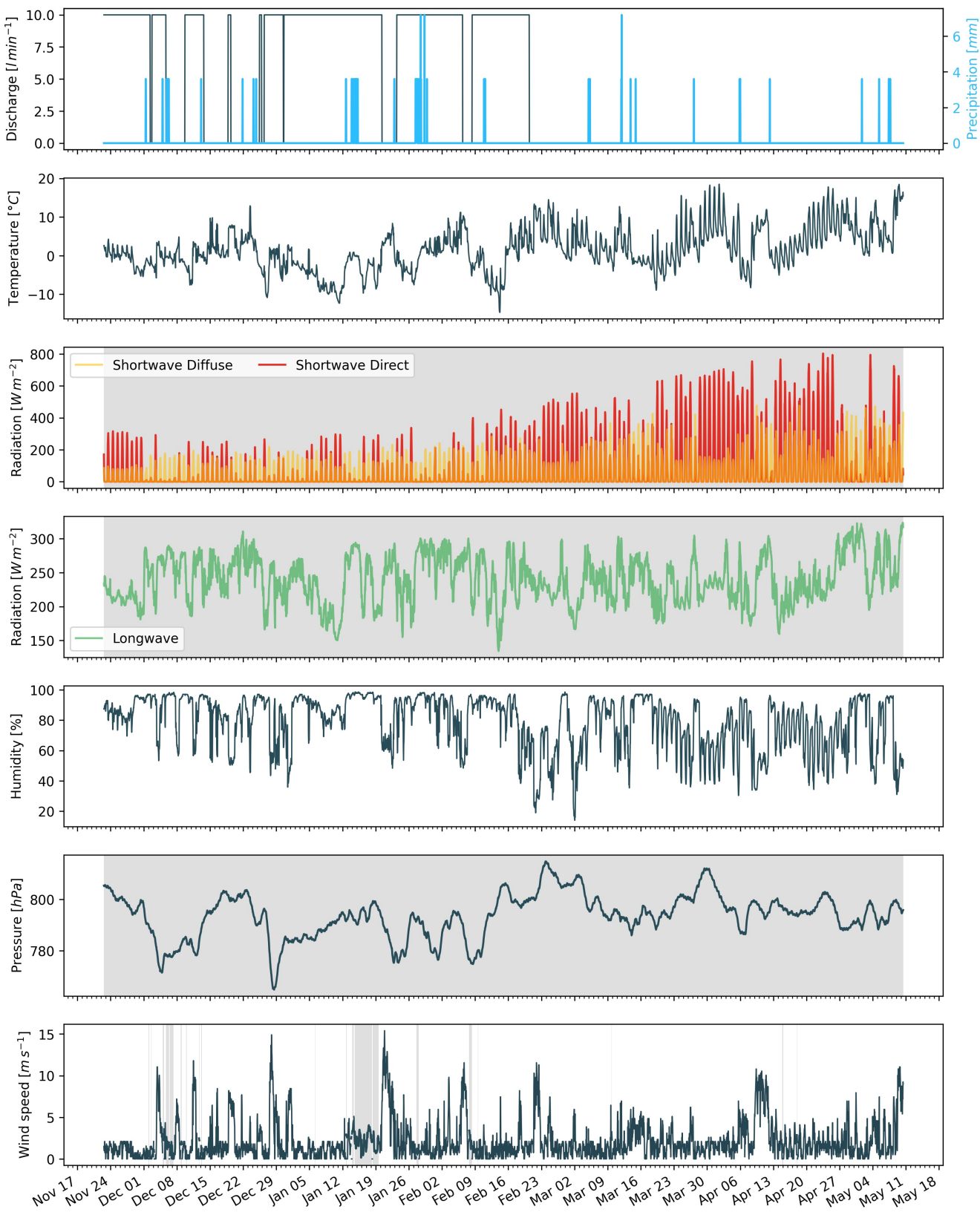


Figure 1. Measurements at the AWS of CH21 were used as main model input data in hourly frequency. Missing data, data gaps and errors were filled from the ERA5 dataset (shaded regions).

42 validation of the model. There were no drone flights conducted for CH19 AIR, so the r_{spray} was instead
 43 calculated from fountain attributes as described in Appendix.

44

AIR	Gangles, 2021	Guttannen, 2021	Guttannen, 2020	Schwarzsee, 2019
Code	IN21	CH21	CH20	CH19
Altitude [m a.s.l.]	4025	1047	1047	967
Construction Team	Icestupa Competition	Guttannen Bewegt	Guttannen Bewegt	Eispalast
Fountain Duration	Jan 18 - Mar 10	Nov 22 - Feb 21	Jan 3 - Feb 27	Jan 30 - Feb 16
Drone Flights	6	9	3	0
r_{spray} [m]	10.8	6.9	7.7	1.2
V_{dome} [m^3]	78.5	13.2	23.9	0

45

2 MODEL SETUP

46 A bulk energy and mass balance model is used to calculate the amounts of ice, meltwater, water vapour
 47 and runoff water of the AIR every hour. This model consists of four modules which estimates the AIR, a)
 48 geometric evolution , b) energy balance, c) surface temperature and d) mass balance.

49 **2.1 Geometric evolution**

50 Radius r_{ice}^i and height h_{ice}^i define the dimensions of the AIR assuming its geometry to be a cone. The
 51 surface area A^i exposed to the atmosphere and volume V^i are:

$$A = \pi \cdot r_{ice} \cdot \sqrt{r_{ice}^2 + h_{ice}^2} \quad (1)$$

$$V = \pi/3 \cdot r_{ice}^2 \cdot h_{ice} \quad (2)$$

52 Note that we do not specify the time step superscript i of the shape variables A , V , r_{ice} and h_{ice} for
 53 brevity. The equations used henceforth display model time step superscript i only if it is different from the
 54 current time step.

55 With the mass of the AIR M_{ice} , its current volume can also be expressed as:

$$V = M_{ice}/\rho_{ice} \quad (3)$$

56 where ρ_{ice} is the density of ice (917 kg m^{-3}).

57 The influence of the AIR fountain is parameterised by the fountain water temperature T_w and its spray
 58 radius r_{spray} . The initial radius r_0 of the AIR is assumed to be r_{spray} . The initial height h_0 depends on the
 59 dome volume V_{dome} used to construct the AIR as follows:

$$h_0 = \Delta x + \frac{3 \cdot V_{dome}}{\pi r_{spray}^2} \quad (4)$$

60 where Δx is the surface layer thickness (defined in Section 2.2)

61 During subsequent time steps, the dimensions of the AIR evolve assuming a uniform ice formation and
 62 decay across its surface area with an invariant slope $s_{cone} = \frac{h_{ice}}{r_{ice}}$. During these time steps, the volume is
 63 parameterised using Eqn. 2 as:

$$V = \frac{\pi \cdot r_{ice}^3 \cdot s_{cone}}{3} \quad (5)$$

64 However, the Icestupa cannot outgrow the maximum range of the water droplets ($(r_{ice})_{max} = r_F$).
 65 Combining equations 2, 4, 3 and 5, the geometric evolution of the Icestupa at each time step i can be
 66 determined by considering the following rules:

$$(r_{ice}, h_{ice}) = \begin{cases} (r_{spray}, h_0) & \text{if } i = 0 \\ (r_{ice}^{i-1}, \frac{3 \cdot M_{ice}}{\pi \cdot \rho_{ice} \cdot (r_{ice}^{i-1})^2}) & \text{if } r_{ice}^{i-1} \geq r_F \text{ and } \Delta M_{ice} > 0 \\ (\frac{3 \cdot M_{ice}}{\pi \cdot \rho_{ice} \cdot s_{cone}})^{1/3} \cdot (1, s_{cone}) & \text{otherwise} \end{cases} \quad (6)$$

67 where $\Delta M_{ice} = M_{ice}^{i-1} - M_{ice}^{i-2}$

68 2.2 Energy Balance

69 The energy balance equation (Hock, 2005) for the AIR is formulated as follows:

$$q_{SW} + q_{LW} + q_L + q_S + q_F + q_G = q_{surf} \quad (7)$$

70 where q_{surf} is the surface energy flux in $[W\ m^{-2}]$; q_{SW} is the net shortwave radiation; q_{LW} is the net
 71 longwave radiation; q_L and q_S are the turbulent latent and sensible heat fluxes. q_F represents the heat
 72 exchange of the fountain water droplets with the AIR ice surface. q_G represents ground heat flux between
 73 Icestupa surface and Icestupa interior. Energy transferred in the direction of the ice surface is always
 74 denoted as positive and away as negative.

75 Equation 7 is usually referred to as the energy budget for “the surface”, but practically it must apply
 76 to a surface layer of ice with a finite thickness Δx . The energy flux acts upon the Icestupa surface layer
 77 which has an upper and a lower boundary defined by the atmosphere and the ice body of the Icestupa,
 78 respectively. The parameter selection for Δx is based on the following two arguments: (a) the ice thickness
 79 Δx should be small enough to represent the surface temperature variations every model time step Δt and
 80 (b) Δx should be large enough for these temperature variations to not reach the bottom of the surface layer.
 81 Therefore, we introduced a 20 mm thick surface layer for a model time step of 1 hour, over which the
 82 energy balance is calculated. A sensitivity analysis was later performed to understand the influence of this
 83 factor. Here, we define the surface temperature T_{ice} to be the modelled average temperature of the Icestupa
 84 surface layer and the energy flux q_{surf} is assumed to act uniformly across the Icestupa area A .

85 2.2.1 Net Shortwave Radiation q_{SW}

86 The net shortwave radiation q_{SW} is computed as follows:

$$q_{SW} = (1 - \alpha) \cdot (SW_{direct} \cdot f_{cone} + SW_{diffuse}) \quad (8)$$

87 where SW_{direct} and $SW_{diffuse}$ are the ERA5 direct and diffuse short wave radiation, α is the modelled
 88 albedo and f_{cone} is the area fraction of the ice structure exposed to the direct shortwave radiation.

89 We model the albedo using a scheme described in Oerlemans and Knap (1998). The scheme records the
 90 decay of albedo with time after fresh snow is deposited on the surface. δt records the number of time steps
 91 after the last snowfall event. After snowfall, albedo changes over a time step, δt , as

$$\alpha = \alpha_{ice} + (\alpha_{snow} - \alpha_{ice}) \cdot e^{(-\delta t)/\tau} \quad (9)$$

92 where α_{ice} is the bare ice albedo value (0.35), α_{snow} is the snow ice albedo value (0.85) and τ is a decay
 93 rate, which determines how fast the albedo of the ageing snow reaches this value. The decay rate τ is
 94 assumed to have a base value of 10 days similar to values obtained by Schmidt et al. (2017) for wet surfaces
 95 and its maximal value is set based on observations by Oerlemans and Knap (1998) as shown in Table 1.
 96 Furthermore, the albedo α varies depending on the water source that formed the current Icestupa surface.
 97 Correspondingly, the albedo is reset to the value of bare ice albedo if the fountain is spraying water onto
 98 the current ice surface and to the value of fresh snow albedo if a snowfall event occurred. Snowfall events
 99 are assumed if the air temperature is below $T_{ppt} = 1^{\circ}C$ (Fujita and Ageta, 2000).

100 The area fraction f_{cone} of the ice structure exposed to the direct shortwave radiation depends on the
 101 shape considered. The direct solar radiation incident on the AIR surface is first decomposed into horizontal
 102 and vertical components using the solar elevation angle θ_{sun} . For a conical shape, half of the total curved
 103 surface is exposed to the vertical component of the direct shortwave radiation and the projected triangle
 104 of the curved surface is exposed to the horizontal component of the direct shortwave radiation. The solar
 105 elevation angle θ_{sun} used is modelled using the parametrisation proposed by Woolf (1968). Accordingly,
 106 f_{cone} is determined as follows:

$$f_{cone} = \frac{(0.5 \cdot r_{ice} \cdot h_{ice}) \cdot \cos\theta_{sun} + (\pi \cdot r_{ice}^2 / 2) \cdot \sin\theta_{sun}}{\pi \cdot r_{ice} \cdot (r_{ice}^2 + h_{ice}^2)^{1/2}} \quad (10)$$

107 The ERA5 diffuse shortwave radiation is assumed to impact the conical Icestupa surface uniformly.

2.2.2 Net Longwave Radiation q_{LW}

109 The net longwave radiation q_{LW} is determined as follows:

$$q_{LW} = LW_{in} - \sigma \cdot \epsilon_{ice} \cdot (T_{ice} + 273.15)^4 \quad (11)$$

110 where T_a represents the measured air temperature, T_{ice} is the modelled surface temperature, both
 111 temperatures are given in $^{\circ}C$, $\sigma = 5.67 \cdot 10^{-8} J m^{-2} s^{-1} K^{-4}$ is the Stefan-Boltzmann constant, LW_{in}
 112 denotes the incoming longwave radiation derived from the ERA5 dataset and ϵ_{ice} is the corresponding
 113 emissivity value for the Icestupa surface (see Table 1).

2.2.3 Turbulent sensible q_S and latent q_L heat fluxes

115 The turbulent sensible q_S and latent heat q_L fluxes are computed with the following expressions proposed
 116 by Garratt (1992):

$$q_S = c_a \cdot \rho_a \cdot p_a / p_{0,a} \cdot \frac{\kappa^2 \cdot v_a \cdot (T_a - T_{ice})}{(\ln \frac{h_{AWS}}{z_{ice}})^2} \quad (12)$$

$$q_L = 0.623 \cdot L_s \cdot \rho_a / p_{0,a} \cdot \frac{\kappa^2 \cdot v_a (p_{v,a} - p_{v,ice})}{\left(\ln \frac{h_{AWS}}{z_{ice}}\right)^2} \quad (13)$$

117 where h_{AWS} is the measurement height above the ground surface of the AWS (in m), v_a is the wind
 118 speed in $[m s^{-1}]$, c_a is the specific heat of air at constant pressure ($1010 J kg^{-1} K^{-1}$), ρ_a is the air density
 119 at standard sea level ($1.29 kg m^{-3}$), $p_{0,a}$ is the air pressure at standard sea level ($1013 hPa$), κ is the
 120 von Karman constant (0.4), L_s is the heat of sublimation ($2848 kJ kg^{-1}$) and z_{ice} ($1.7 mm$) denotes the
 121 roughness length of ice (momentum and scalar). The vapor pressures over air ($p_{v,a}$) and ice ($p_{v,ice}$) was
 122 obtained using the following formulation given in WMO (2018):

$$\begin{aligned} p_{v,a} &= 6.107 \cdot 10^{(7.5 \cdot T_a / (T_a + 237.3))} \\ p_{v,ice} &= (1.0016 + 3.15 \cdot 10^{-6} \cdot p_a - 0.074 \cdot p_a^{-1}) \cdot (6.112 \cdot e^{(22.46 \cdot T_{ice} / (T_{ice} + 272.62))}) \end{aligned} \quad (14)$$

123 where p_a is the measured air pressure in [hPa].

2.2.4 Fountain water heat flux q_F

124 The interaction between the fountain water and the ice surface is taken into account by assuming that
 125 the ice surface temperature remains constant at $0 ^\circ C$ during time steps when the fountain is active. This
 126 process can be divided into two simultaneous steps: (a) the water temperature T_{water} is cooled to $0 ^\circ C$
 127 and (b) the ice surface temperature is warmed to $0 ^\circ C$. Process (a) transfers the necessary energy for
 128 process (b) throughout the fountain runtime. We further assume that this process is instantaneous, i.e. the
 129 ice temperature is immediately set to $0 ^\circ C$ within just one time step Δt when the fountain is switched on.
 130 Thus, the heat flux caused by the fountain water is calculated as follows:

$$q_F = \begin{cases} 0 & \text{if } \Delta M_F = 0 \\ \frac{\Delta M_F \cdot c_{water} \cdot T_{water}}{\Delta t \cdot A} + \frac{\rho_{ice} \cdot \Delta x \cdot c_{ice} \cdot T_{ice}}{\Delta t} & \text{if } \Delta M_F > 0 \end{cases} \quad (15)$$

132 with c_{ice} as the specific heat of ice.

2.2.5 Bulk Icestupa heat flux q_G

133 The bulk Icestupa heat flux q_G corresponds to the ground heat flux in normal soils and is caused by the
 134 temperature gradient between the surface layer (T_{ice}) and the ice body (T_{bulk}). It is expressed by using the
 135 heat conduction equation as follows:

$$q_G = k_{ice} \cdot (T_{bulk} - T_{ice}) / l_{ice} \quad (16)$$

137 where k_{ice} is the thermal conductivity of ice ($2.123 W m^{-1} K^{-1}$), T_{bulk} is the mean temperature of the
 138 ice body within the Icestupa and l_{ice} is the average distance of any point in the surface to any other point in
 139 the ice body. T_{bulk} is initialised as $0 ^\circ C$ and later determined from Eqn. 16 as follows:

$$T_{bulk}^{i+1} = T_{bulk} - (q_G \cdot A \cdot \Delta t) / (M_{ice} \cdot c_{ice}) \quad (17)$$

Table 1. Free parameters in the model categorised as constant, uncertain and site parameters. Base value (B) and uncertainty (U) were taken from the literature. For assumptions (assum.), the uncertainty was chosen to be relatively large (5 %). For measurements (meas.), the uncertainty due to parallax errors is chosen to be (1 %).

Constant Parameters	Symbol	Value	References
Van Karman constant	κ	0.4	B: Cuffey and Paterson
Stefan Boltzmann constant	σ	$5.67 \cdot 10^{-8} W m^{-2} K^{-4}$	B: Cuffey and Paterson
Air pressure at sea level	$p_{0,a}$	1013 hPa	B: Mölg and Hardy
Density of water	ρ_w	$1000 kg m^{-3}$	B: Cuffey and Paterson
Density of ice	ρ_{ice}	$917 kg m^{-3}$	B: Cuffey and Paterson
Density of air	ρ_a	$1.29 kg m^{-3}$	B: Mölg and Hardy
Specific heat of ice	c_{ice}	$2097 J kg^{-1} ^\circ C^{-1}$	B: Cuffey and Paterson
Specific heat of water	c_w	$4186 J kg^{-1} ^\circ C^{-1}$	B: Cuffey and Paterson
Specific heat of air	c_a	$1010 J kg^{-1} ^\circ C^{-1}$	B: Mölg and Hardy
Thermal conductivity of ice	k_{ice}	$2.123 W m^{-1} K^{-1}$	B: Bonales et al.
Latent Heat of Sublimation	L_s	$2848 kJ kg^{-1}$	B: Cuffey and Paterson
Latent Heat of Fusion	L_f	$334 kJ kg^{-1}$	B: Cuffey and Paterson
Uncertain Parameters		Range	
Precipitation	T_{ppt}	$1 ^\circ C$	$\pm 1 ^\circ C$
Temperature threshold			B + U: Fujita and Ageta, Zhou et al.
Ice Emissivity	ϵ_{ice}	0.95	[0.949,0.993]
Ice Albedo	α_{ice}	0.35	$\pm 5 \%$
Snow Albedo	α_{snow}	0.85	$\pm 5 \%$
Albedo Decay Rate	τ	10 days	[1, 22] days
Surface layer thickness	Δx	20 mm	[1, 10] mm
Fountain Parameters		Range	
Spray Radius	r_{spray}		$\pm 5 \%$
Water temperature	T_{water}	$1 ^\circ C$	[0, 5] $^\circ C$

140 Since AIR's typically have conical shapes with $r_{ice} >> h_{ice}$, we assume that the center of mass of the ice
 141 body is near the base of the fountain. Thus, the distance of every point in the AIR surface layer from the ice
 142 body's center of mass is between h_{ice} and r_{ice} . So we calculate q_G here assuming $l_{ice} = (r_{ice} + h_{ice})/2$.

2.3 Surface temperature

144 The available energy q_{surf} can act on the surface of the AIR to a) change its temperature, b) melt ice or
 145 c) freeze ice. So Eqn. 7 can be rewritten as:

$$q_{surf} = q_{freeze/melt} + q_T \quad (18)$$

146 where q_T , q_{freeze} and q_{melt} represent energy associated with process (a), (b) and (c) respectively.

147 To distribute the surface energy flux into these three components, we categorize the model time steps
 148 as freezing or melting events. Freezing events can only occur if there is fountain water available and the
 149 surface energy flux is negative. But just these two conditions are not sufficient as the latent heat energy

150 can only contribute to temperature fluctuations. So to prevent latent heat energy from turning a melting
 151 event into a freezing event an additional condition namely $(q_{surf} - q_L) < 0$ is required. Thus, freezing and
 152 melting events are identified as follows:

$$q_{freeze/melt} = \begin{cases} q_{freeze} & \text{if } \Delta M_F > 0 \text{ and } q_{surf} < 0 \text{ and } (q_{surf} - q_L) < 0 \\ q_{melt} & \text{otherwise} \end{cases} \quad (19)$$

153 During a freezing event, the available energy $(q_{surf} - q_L)$ can either be sufficient or insufficient to
 154 freeze the fountain water available. If insufficient, the additional energy further cools down the surface
 155 temperature. So the surface energy flux distribution during a freezing event can be represented as:

$$(q_{freeze}, q_T) = \begin{cases} (q_{surf} - q_L, q_L) & \text{if } \Delta M_F \geq -\frac{(q_{surf} - q_L)A \cdot \Delta t}{L_f} \\ \left(\frac{\Delta M_F \cdot L_f}{A \cdot \Delta t}, q_{surf} + \frac{\Delta M_F \cdot L_f}{A \cdot \Delta t}\right) & \text{if } \Delta M_F < -\frac{(q_{surf} - q_L)A \cdot \Delta t}{L_f} \end{cases} \quad (20)$$

156 During a melting event, the surface energy flux (q_{surf}) is first used to change the surface temperature to
 157 T_{temp} calculated as:

$$T_{temp} = \frac{q_{surf} \cdot \Delta t}{\rho_{ice} \cdot c_{ice} \cdot \Delta x} + T_{ice} \quad (21)$$

158 If $T_{temp} > 0^\circ C$, then energy is reallocated from q_T to q_{melt} to maintain surface temperature at melting
 159 point. So the surface energy flux distribution during a melting event can be represented as:

$$(q_{melt}, q_T) = \begin{cases} (0, q_{surf}) & \text{if } T_{temp} < 0 \\ \left(\frac{T_{temp} \cdot \rho_{ice} \cdot c_{ice} \cdot \Delta x}{\Delta t}, q_{surf} - \frac{T_{temp} \cdot \rho_{ice} \cdot c_{ice} \cdot \Delta x}{\Delta t}\right) & \text{if } T_{temp} > 0 \end{cases} \quad (22)$$

160 2.4 Mass Balance

161 The mass balance equation for an AIR is represented as:

$$\frac{\Delta M_F + \Delta M_{ppt} + \Delta M_{dep}}{\Delta t} = \frac{\Delta M_{ice} + \Delta M_{water} + \Delta M_{sub} + \Delta M_{runoff}}{\Delta t} \quad (23)$$

162 where M_F is the discharge of the fountain; M_{ppt} is the cumulative precipitation; M_{dep} is the cumulative
 163 accumulation through water vapour deposition; M_{ice} is the cumulative mass of ice; M_{water} is the cumulative
 164 mass of melt water; M_{sub} represents the cumulative water vapor loss by sublimation and M_{runoff} represents
 165 the fountain discharge runoff that did not interact with the AIR. The LHS of equation 23 represents the rate
 166 of mass input and the RHS represents the rate of mass output for an AIR.

167 Precipitation input is calculated as shown in equation 24a where ρ_w is the density of water (1000
 168 $kg m^{-3}$), ppt is the measured precipitation rate in [$m s^{-1}$] and T_{ppt} is the temperature threshold below
 169 which precipitation falls as snow. Here, snowfall events were identified using T_{ppt} as $1^\circ C$. Snow mass
 170 input is calculated by assuming a uniform deposition over the entire circular footprint of the Icestupa.

171 The latent heat flux is used to estimate either the evaporation and condensation processes or sublimation
 172 and deposition processes as shown in equation 24b. During time steps at which surface temperature is
 173 below $0^\circ C$ only sublimation and deposition can occur, but if the surface temperature reaches $0^\circ C$,

174 evaporation and condensation can also occur. As the differentiation between evaporation and sublimation
 175 (and condensation and deposition) when the air temperature reaches 0 °C is challenging, we assume
 176 that negative (positive) latent heat fluxes correspond only to sublimation (deposition), i.e. no evaporation
 177 (condensation) is calculated.

178 Since we have categorized every time step as a freezing and melting event, we can determine the meltwater
 179 and ice generated using the associated energy fluxes as shown in equations 24c and 24d. Having calculated
 180 all the other mass components the fountain wastewater generated every time step can be calculated using
 181 equation 24e.

$$\frac{\Delta M_{ppt}}{\Delta t} = \begin{cases} \pi \cdot r_{ice}^2 \cdot \rho_w \cdot ppt & \text{if } T_a < T_{ppt} \\ 0 & \text{if } T_a \geq T_{ppt} \end{cases} \quad (24a)$$

$$\left(\frac{\Delta M_{dep}}{\Delta t}, \frac{\Delta M_{sub}}{\Delta t} \right) = \begin{cases} \frac{q_L \cdot A}{L_s} \cdot (1, 0) & \text{if } q_L \geq 0 \\ \frac{q_L \cdot A}{L_s} \cdot (0, -1) & \text{if } q_L < 0 \end{cases} \quad (24b)$$

$$\frac{\Delta M_{water}}{\Delta t} = \frac{q_{melt} \cdot A}{L_f} \quad (24c)$$

$$\frac{\Delta M_{ice}}{\Delta t} = \frac{q_{freeze} \cdot A}{L_f} + \frac{\Delta M_{ppt}}{\Delta t} + \frac{\Delta M_{dep}}{\Delta t} - \frac{\Delta M_{sub}}{\Delta t} - \frac{\Delta M_{melt}}{\Delta t} \quad (24d)$$

$$\frac{\Delta M_{runoff}}{\Delta t} = \frac{\Delta M_F - \Delta M_{ice}}{\Delta t} \quad (24e)$$

182 Considering AIRs as water reservoirs, we can quantify their potential through the amount of water they
 183 store (storage quantity) and the length of time they store it (storage duration). Another means of comparing
 184 different Icestupas is through their water storage efficiency defined accordingly as:

$$\text{Storage Efficiency} = \frac{M_{water}}{(M_F + M_{ppt} + M_{dep})} \cdot 100 \quad (25)$$

3 MODEL RESULTS

185 The model was forced with meteorological data from 30th January to 5th April 2019 (Fig. 1) and various
 186 parameters (see Table 1) to calculate the mass and energy balance of the Icestupa.

187 3.1 Energy and mass balance calculation

188 Daily averages of some components of the energy balance are shown in Fig. 2 (b). On average during
 189 the experiment duration, the total energy balance was almost zero. Net shortwave radiation (33 W m⁻²),
 190 sensible (10 W m⁻²) and latent heat flux (2 W m⁻²) with a mostly positive flux towards the surface of the
 191 icestupa were compensated by the surf longwave radiation (- 34 W m⁻²) and the melt energy (-12 W m⁻²).
 192 The contributions of other fluxes were negligible in comparison.

193 Net shortwave radiation is the main input to, and the most varying energy flux on the ice surface. Its
 194 variability is controlled by the surface albedo α and the area fraction f_{cone} which therefore represent key
 195 variables in the energy balance (Fig. ?? (b)). Although global radiation flux reached a daily maximum
 196 value of 339 W m⁻², q_{SW} only went up to 98 W m⁻². This is caused by the fact that only about 30 % of
 197 the direct solar radiation influenced the Icestupa surface as shown by the area fraction f_{cone} in Fig. ?? (a).

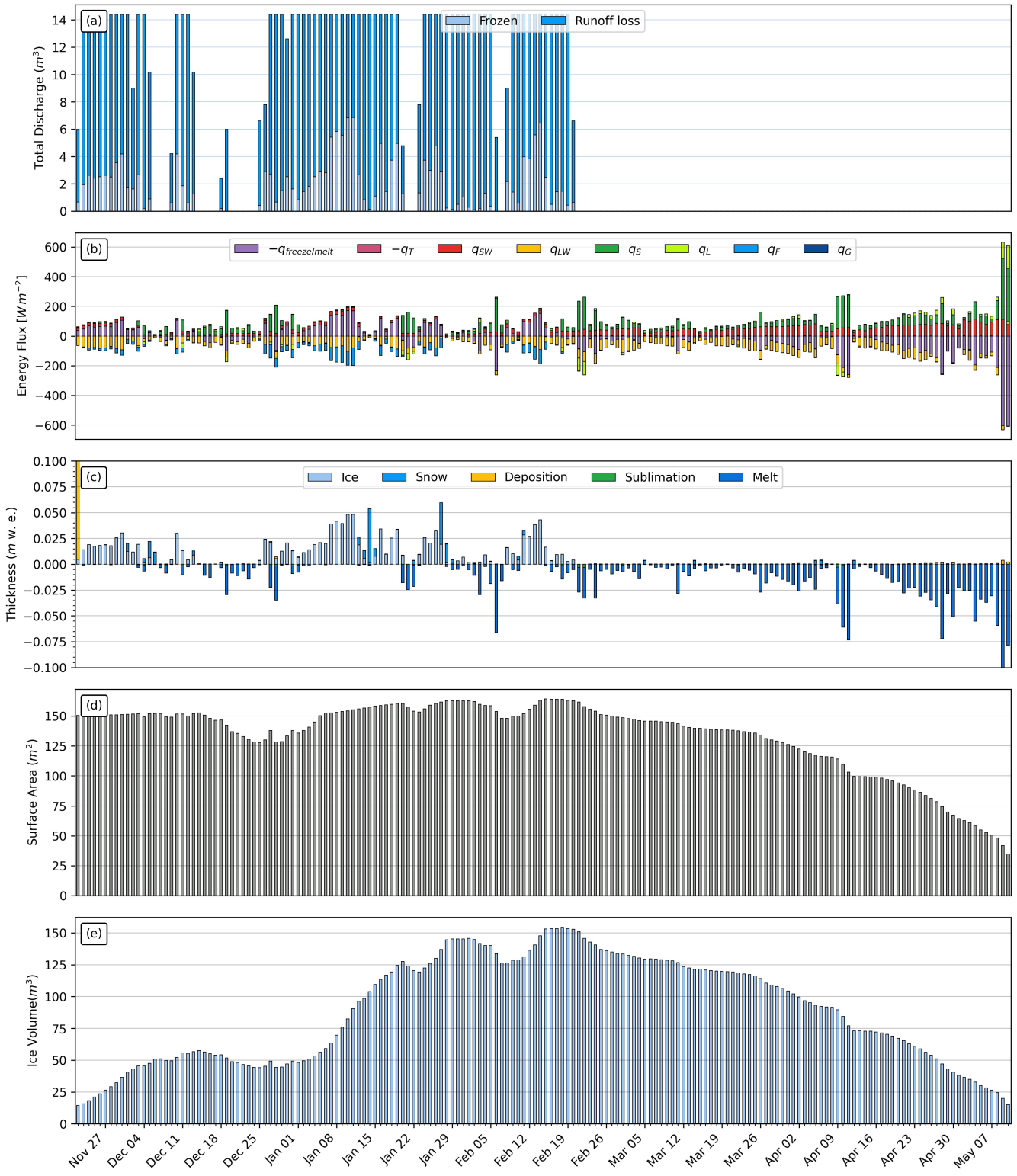


Figure 2. (a) Fountain discharge (b) energy flux components, (c) mass flux components (d) surface area and (e) volume of the Icestupa in daily time steps. q_{SW} is the net shortwave radiation; q_{LW} is the net longwave radiation; q_L and q_S are the turbulent latent and sensible heat fluxes. q_F represents the interactions of the fountain water with the AIR surface layer. q_G quantifies the heat conduction process between the AIR surface layer and the ice body.

Table 2. Summary of mass balance components for the CH21 experiment after the fountain spray was stopped (on 15th February 2019) and at the end of the model run (on 5th April). All parameters except M_F were modelled.

	Mass Component	Model ends
Input	M_F	1,000,041 kg
	M_{ppt}	29,533 kg
	M_{dep}	4,755 kg
Output	M_{water}	196,011 kg
	M_{ice}	12,304 kg
	M_{sub} M_{runoff}	4,747 kg 821,267 kg

198 Snowfall is the atmospheric variable connected most closely and proportionally to albedo. Higher and/or
 199 more frequent snowfall thus decreases the energy available for melt due to the corresponding increase in α .

200 q_{LW} was predominantly negative indicating that this energy balance component drove the freezing of
 201 the ice structure. Daily values of q_{LW} ranged from -89 to 21 Wm^{-2} . Turbulent sensible heat flux q_S
 202 contributed mostly to the melt of the ice structure. Daily values of q_S ranged from -14 to 26 Wm^{-2} .
 203 Deposition/condensation was favored over evaporation/sublimation during 95 % of the model runtime.
 204 Daily values of the turbulent latent heat flux q_L ranged from -10 to 15 Wm^{-2} . Since the mean of q_L was
 205 positive, the Icestupa gained mass cumulatively from the atmosphere due to the condensation process.
 206 Fountain water heat flux q_F had a mean of zero as it was only nonzero during 1002 time steps or around
 207 100 hours. Daily values of q_F ranged from -1 to 6 Wm^{-2} . The contribution of heat flux by conduction
 208 q_G was also minimal as it only varied between -6 to 12 Wm^{-2} with a mean of 0 Wm^{-2} . The energy
 209 contributing to surface temperature changes (q_T) was insignificant in comparison to the energy spent on
 210 freezing and melting (q_{melt}). The resulting bulk temperature and the surface temperature are shown in Fig.
 211 ?? (b). For the total considered period, q_{LW} accounted for 33.8% of overall energy turnover. The energy
 212 turnover is calculated as the sum of energy fluxes in absolute values. q_{SW} accounted for 31.3%, followed
 213 by q_{melt} (19%), q_S (9.6%), q_L (3.6%), q_G (2.4%), q_F (0.2%) and q_T (0.4%).

214 Fig. 2 (c) represents the mass fluxes associated with these energy exchanges expressed in m w.e. It
 215 shows the ice and meltwater formed due to q_{melt} , snow accumulated due to precipitation, water vapour
 216 deposition/condensation and sublimation/evaporation due to q_L . Growth rate ($\frac{\Delta M_{ice}}{\Delta t}$) shows a better
 217 correlation with surf energy flux ($r^2 = 0.15$) compared to Icestupa surface area ($r^2 = 0.04$). This is
 218 because the variance in growth rate is mostly due to the variance in q_{surf} as illustrated in Fig. 2. Since r_{ice}
 219 was initialised with the spray radius r_{spray} , the surface area maintains a maximum initially until the energy
 220 flux becomes positive. This trend favours the positive over the negative thickness changes resulting in a
 221 steep increase and gradual melting of ice volume as can be seen in Fig. ??.

222 The total water used for the Icestupa development includes contributions from the fountain (97.3%),
 223 snowfall (2.5 %), condensation (0.2 %) as shown in Table 2. The maximum ice mass during the whole
 224 measurement period was 809 kg, which occurred after the last fountain run on Feb 16th 2019 in the
 225 morning. Therefore, in the case of CH21 we used a water input of 18,558 kg, with a resultant storage
 226 efficiency of only 5.5 %.

REFERENCES

- 227 Bonales, L. J., Rodriguez, A. C., and Sanz, P. D. (2017). Thermal conductivity of ice prepared under
228 different conditions. *International Journal of Food Properties* 20, 610–619. doi:10.1080/10942912.
229 2017.1306551
- 230 [Dataset] Copernicus Climate Change Service (C3S) (2017). Era5: Fifth generation of ecmwf atmospheric
231 reanalyses of the global climate. [Available at <https://cds.climate.copernicus.eu/cdsapp#!/home>, accessed 2019-10-01]
- 233 Cuffey, K. M. and Paterson, W. S. B. (2010). *The Physics Of Glaciers* (Elsevier)
- 234 Fujita, K. and Ageta, Y. (2000). Effect of summer accumulation on glacier mass balance on the
235 tibetan plateau revealed by mass-balance model. *Journal of Glaciology* 46, 244–252. doi:10.3189/172756500781832945
- 237 Garratt, J. R. (1992). *The Atmospheric Boundary Layer* (Cambridge University Press)
- 238 Hock, R. (2005). Glacier melt: a review of processes and their modelling. *Progress in Physical Geography: Earth and Environment* 29, 362–391
- 240 Hori, M., Aoki, T., Tanikawa, T., Motoyoshi, H., Hachikubo, A., Sugiura, K., et al. (2006). In-situ
241 measured spectral directional emissivity of snow and ice in the 8–14 micrometer atmospheric window.
242 *Remote Sensing of Environment* 100, 486 – 502
- 243 Mölg, T. and Hardy, D. R. (2004). Ablation and associated energy balance of a horizontal glacier surface
244 on kilimanjaro. *J. Geophys. Res.-Atmos.* 109, 1–13. doi:10.1029/2003JD004338
- 245 Oerlemans, J. and Knap, W. H. (1998). A 1 year record of global radiation and albedo in the
246 ablation zone of morteratschletscher, switzerland. *Journal of Glaciology* 44, 231–238. doi:10.3189/S0022143000002574
- 248 Scherrer, S. C. (2020). Temperature monitoring in mountain regions using reanalyses: lessons from the
249 alps. *Environmental Research Letters* 15, 044005
- 250 Schmidt, L. S., Aðalgeirs Þóttir, G., Guðmundsson, S., Langen, P. L., Pálsson, F., Mottram, R., et al. (2017).
251 The importance of accurate glacier albedo for estimates of surface mass balance on vatnajökull: evaluating
252 the surface energy budget in a regional climate model with automatic weather station observations. *The Cryosphere* 11, 1665–1684. doi:10.5194/tc-11-1665-2017
- 254 WMO (2018). *Guide to Instruments and Methods of Observation* (World Meteorological Organization ;
255 2018 (2018 Edition))
- 256 Woolf, H. M. (1968). *On the Computation of Solar Elevation Angles and the determination of sunrise and
257 sunset times* (National Aeronautics and Space Administration)
- 258 Zhou, S., Kang, S., Gao, T., and Zhang, G. (2010). Response of zhadang glacier runoff in nam co basin,
259 tibet, to changes in air temperature and precipitation form. *Chinese Science Bulletin* 55, 2103–2110.
260 doi:10.1007/s11434-010-3290-5